
Accelerating Distributed Deep Learning using Lossless Homomorphic Compression

Haoyu Li¹ Yuchen Xu² Jiayi Chen¹ Rohit Dwivedula¹ Wenfei Wu² Keqiang He³ Aditya Akella¹
Daebyeok Kim¹

Abstract

As deep neural networks (DNNs) grow in complexity and size, the resultant increase in communication overhead during distributed training has become a significant bottleneck, challenging the scalability of distributed training systems. Existing solutions, while aiming to mitigate this bottleneck through worker-level compression and in-network aggregation, fall short due to their inability to efficiently reconcile the trade-offs between compression effectiveness and computational overhead, hindering overall performance and scalability. In this paper, we introduce a novel compression algorithm that effectively merges worker-level compression with in-network aggregation. Our solution is both homomorphic, allowing for efficient in-network aggregation without CPU/GPU processing, and lossless, ensuring no compromise on training accuracy. Theoretically optimal in compression and computational efficiency, our approach is empirically validated across diverse DNN models such as NCF, LSTM, VGG19, and BERT-base, showing up to a $6.33\times$ improvement in aggregation throughput and a $3.74\times$ increase in per-iteration training speed.

1. Introduction

Deep neural networks (DNNs) have been rapidly growing in size due to the increase in computing power and availability of large datasets. Models like BERT-base and BERT-large have 110 million and 340 million parameters respectively (Devlin et al., 2018), while GPT-3 boasts an impressive 175 billion parameters (Brown et al., 2020). Larger models can capture a wider range of high-level features, leading to advances in fields such as image and natural language processing and recommendation systems (He et al., 2016; Yin et al., 2017; Gupta et al., 2020).

Distributed training using data parallelism (Ben-Nun and Hoefler, 2019) is a standard approach for large DNN models. Local gradients are computed through stochastic gradient descent (SGD) (Bottou et al., 2018) by multiple workers, and then aggregated (summed up) globally using either a centralized parameter server (Li et al., 2014; Luo et al., 2018; Jiang et al., 2020) or a decentralized AllReduce approach (Barnett et al., 1994; Chan et al., 2007; Patarasuk and Yuan, 2009).

However, it is challenging to aggregate gradients due to the large volume of traffic generated, particularly when network bandwidth is limited. This can create a bottleneck, especially when dealing with large models. For instance, it takes almost half the time for aggregation when training BERT-base with eight workers (Devlin et al., 2018). Furthermore, GPU computation throughput is advancing faster than network bandwidth (Sun et al., 2019), which means that the existing imbalance between computation and communication will continue to grow (Sevilla et al., 2022).

Prior work tackles the communication bottleneck in two ways. First, worker-level compression techniques (Wang et al., 2023) aim to reduce the amount of data being communicated, thereby enabling gradient aggregation at a throughput that exceeds the network bandwidth. However, their compressed data formats often require additional CPU/GPU processing during aggregation, which might offset the speed gains achieved from reduced traffic (Li et al., 2023b). Second, in-network aggregation approaches delegate the aggregation process to network infrastructure components such as programmable hardware switches (Sapio et al., 2021; Lao et al., 2021) and specialized middleboxes (Gebara et al., 2021). They take advantage of high packet processing speeds and bandwidth capabilities of switches and middleboxes, effectively bypassing CPU/GPU involvement and enhancing training throughput (Feng et al., 2023). Nevertheless, this training throughput is strictly bounded by the physical network bandwidth, and the constraint makes it increasingly difficult to address the growing imbalance between computation and communication.

It is tantalizing to combine and harness the benefits of both to optimize communication; however, these two approaches encounter inherent conflicts primarily stemming from hardware limitations (Li et al., 2023b), making their seamless

¹UT Austin. ²Peking University. ³Airbnb. Correspondence to: Haoyu Li <lhy@utexas.edu>, Aditya Akella <akella@cs.utexas.edu>, Daebyeok Kim <daebyeok@utexas.edu>.

integration challenging. Compression algorithms usually do not support for aggregation after compression, referred to as “homomorphic compression” (Li et al., 2023b; Jang et al., 2017)¹. Even for those that do, such as Sketched-SGD (Ivkin et al., 2019), the use of probabilistic data structures inevitably introduces accuracy loss. This loss may necessitate additional iterations for the model to converge, potentially undermining the overall training performance (Li et al., 2023b). From the perspective of in-network aggregation, challenges arise when attempting to directly aggregate data compressed in formats like coordinate list, commonly used in compression algorithms.

In this paper, we propose a homomorphic and lossless compression algorithm that can work with in-network gradient aggregation without incurring accuracy loss. At a high level, our algorithm consists of two phases to aggregate gradients: compression and recovery. In the compression phase, each worker encodes the original gradient, denoted as \mathbf{X} , into a homomorphic compressed form, denoted as $\mathcal{S}(\mathbf{X})$, and transmits $\mathcal{S}(\mathbf{X})$ to the existing aggregation API. In the recovery phase, each worker receives the aggregated compressed data, *i.e.*, $\mathcal{S}(\sum \mathbf{X})$, from the aggregation API and accurately recovers $\sum \mathbf{X}$ from it. The novelty of our algorithm hinges on two key techniques. First, we use two homomorphic data structures to construct $\mathcal{S}(\sum \mathbf{X})$ while preserving all information. Second, we utilize a practical algorithm from the field of random graphs for the accurate recovery of the aggregated gradient. To elaborate, our initial step involves compressing the original gradient \mathbf{X} into a homomorphic dimensionality-reducing structure known as Count Sketch (Charikar et al., 2002). Following this, we let $\mathcal{S}(\sum \mathbf{X})$ include not only the Count Sketch but also an additional homomorphic indexing structure. This indexing structure is pivotal in identifying non-zero parameters, thereby mitigating potential estimation errors on zero values. More importantly, we observe that after discarding the zero parameters, the size of non-zero parameters of DNN gradients can be comparable to the size of the Count Sketch. This suggests that Count Sketch operates as a de facto invertible linear transformation instead of a tool for dimensionality reduction, preserving information without any loss. Finally, we discover that an existing algorithm in random graphs, known as parallel peeling (Jiang et al., 2017) can be adeptly applied to recover the aggregated data, and thus achieving the lossless property.

Our algorithm theoretically boasts two compelling features beyond its homomorphic and lossless properties. First, our algorithm achieves a high compression ratio, defined as the size of the original data divided by the size of the compressed data. In fact, for any data type (*e.g.*, 4-bit integer)

¹The term “homomorphic” means the compressed aggregated data is equivalent to the aggregated compressed data.

and any level of sparsity (*e.g.*, when 99% parameters are zero) of the parameters, it guarantees asymptotically optimal use of bottleneck network bandwidth. Second, our algorithm achieves a high computation throughput with linear (asymptotically optimal) computational complexity for compression and decompression. The processes also exhibit good spatial locality, further enhancing their computational efficiency.

We empirically demonstrate a remarkable enhancement in the performance of distributed training across various tasks, including Neural Collaborative Filtering (NCF) (He et al., 2017), Long Short-Term Memory networks (LSTM) (Hochreiter and Schmidhuber, 1997), VGG19 (Simonyan and Zisserman, 2014), and BERT-base (Devlin et al., 2018). We integrate our algorithm into the most popular NVIDIA Collective Communications Library (NCCL) AllReduce framework and the ATP (Lao et al., 2021) in-network aggregation framework in PyTorch (Paszke et al., 2019), finding that compared to the baseline training performance using standard NCCL and ATP, our algorithm achieves up to 6.33 \times speedup in terms of aggregation throughput and 3.74 \times speedup in terms of per iteration training. We have open-sourced our implementation.²

2. Related Work

We overview the two mainstream approaches to mitigate the communication bottleneck: compression and in-network aggregation.

Compression is a method of reducing data volume to decrease communication traffic using two techniques. The first, sparsification, involves filtering out parameters of lesser magnitude before transmission for aggregation. For example, selecting only the top 1% of parameters in terms of absolute value for aggregation does not significantly impact accuracy (Li and Hoefler, 2022). Various studies in sparsification, such as TopkA (Wang et al., 2020), TopkDSA (Renggli et al., 2019), and gTopk (Shi et al., 2019), focus on the efficient selection of either local or global Topk parameters. However, these works generally lack support for aggregation after compression, referred to as the homomorphic property (Jang et al., 2017; Li et al., 2023b), due to their reliance on specific parameter storage formats like the coordinate list. This necessitates decompressing the gradients from all workers, aggregating them, and then compressing again before redistribution, significantly increasing computational overhead and traffic latency (Li et al., 2023b). Even in works like Sketched-SGD (Ivkin et al., 2019), which compress gradients into a homomorphic data structure called Count Sketch, they suffer from accuracy loss due to their

²https://github.com/lihy0529/lossless_homomorphic_compression.

probabilistic nature, leading to more training iterations and reduced model accuracy. Our compression algorithm, in contrast, seeks to maintain accuracy while preserving the homomorphic property. The second key technique in compression is gradient quantization, which involves mapping the value of each parameter to a lower precision range. For example, TernGrad (Wen et al., 2017) shows that mapping each parameter’s value into a two-bit range $\in \{-1, 0, 1\}$ can still preserve training convergence. Similar to sparsification, many quantization studies vary mainly in their bit-width approach, such as FP16 (Micikevicius et al., 2017), 8-Bit (Dettmers, 2015), and SignSGD (Seide et al., 2014). However, as these works are orthogonal to our algorithm, they will not be the focus of our discussion.

In-network aggregation approaches offload the aggregation process to network infrastructure components such as programmable hardware switches and specialized middleboxes. They leverage the high packet processing speed of switches and middleboxes to aggregate up to terabits of parameters per second. This approach mitigates the communication bottleneck by minimizing the traffic that would originally transverse the entire network. Examples of systems employing this method include SwitchML (Sapio et al., 2021) and ATP (Lao et al., 2021). However, in-network aggregation has a significant drawback in the form of hardware restrictions, as switches and middleboxes have a limited number of pipeline stages available for processing fixed-function operations (Li et al., 2023b). This makes it challenging to directly aggregate data in formats other than simple gradient vectors. Even in works like Libra (Pan et al., 2022) which support aggregation after compression, they inevitably incur additional accuracy loss because they cannot proceed all parameters within limited memory on switches. Our compression algorithm, in contrast, seeks to support in-network aggregation on compressed gradients while keeping the lossless property.

3. Algorithm Design

We propose a lossless homomorphic compression algorithm, simultaneously reducing the volume of data to be communicated without information loss, as well as avoiding CPU/GPU involvements during aggregation, thus harnessing the benefits of both compression and in-network aggregation.

At a high level, our algorithm consists of two phases to aggregate gradients (Algorithm 1): compression and recovery. In the compression phase, each worker encodes the original gradient, denoted as X , into a homomorphic compressed form, denoted as $S(X)$, and transmits $S(X)$ to the existing aggregation API such as NCCL AllReduce and ATP in-network aggregation (Lao et al., 2021). In the recovery phase, each worker receives the aggregated compressed

data, *i.e.*, $S(\sum X)$, from the aggregation API and accurately recovers $\sum X$ from it. $S(X)$ comprises two fundamental as well as homomorphic components: a data structure Y called Count Sketch, satisfying $Y(\sum X) = \sum Y(X)$, and a compact indexing structure B , satisfying $B(\sum X) = \vee B(X)$, where \vee represents aggregating gradients with bitwise-OR operation.

Algorithm 1 Lossless Homomorphic Compression

Phase I: Compression

Input: gradient X ;
 Build Count Sketch Y of X ; //§3.1
 Build index B of X ; //§3.2, §3.3
Output: aggregate ($S(X) := [Y, B]$); //API

// The API makes $S(X) \leftarrow S(\sum X)$
 // by making $Y \leftarrow \sum Y$ and $B \leftarrow \vee B$.

Phase II: Recovery

Input: $[Y, B] := S(X)$; //API
 $X \leftarrow \text{peel}(Y, B)$; //§3.2
 Estimate the not recovered parameters of X from Y ;
Output: X ; //Aggregated gradient

This section is structured as follows: In §3.1, we leverage sketching theory (Li et al., 2022) to achieve the homomorphic property. We employ Count Sketch (Charikar et al., 2002), which is pivotal in providing an unbiased estimation of parameters. In §3.2, we leverage peeling theory (Jiang et al., 2017) to achieve the lossless property. We incorporate an additional bitmap index alongside the Count Sketch, accurately reconstructing the parameters from their compressed state. In §3.3, we leverage membership theory (Li et al., 2023a) to achieve a high compression ratio, defined as the size of the original data divided by the size of the compressed data. We theoretically propose using a probabilistic data structure called Bloom Filter (Bloom, 1970) as the additional index, making the compression ratio asymptotically optimal.³ In §3.4, we make the locality optimization to achieve high computation throughput. We substantially reduce the number of memory access by processing consecutive parameters in batches.

3.1. Count Sketch: Homomorphic Compression

Count Sketch (Charikar et al., 2002) is an effective technique for unbiased dimensionality reduction. We start from here because it meets the homomorphic property, *i.e.*, satisfies $\vec{Y}(\sum \vec{X}) = \sum \vec{Y}(\vec{X})$. Specifically, it compresses the original \vec{X} into an array \vec{Y} in the following manner: Each index i of \vec{X} is hashed to three signals $g_1(i), g_2(i), g_3(i) \in \{-1, 1\}$, and three different indexes $h_1(i), h_2(i), h_3(i)$ in \vec{Y} . The Count Sketch process involves incrementing the $h_j(i)$ -th ($j = 1, 2, 3$) parameter in \vec{Y} by $(g_j(i) \cdot x_i)$, which results

³This is only theoretically necessary when the sparsity is extremely high.

in either X_i or $-X_i$, depending on the signal $g_j(i)$. To estimate aggregated gradient \vec{X} , the worker examines the mapped value $Y_{h_j(i)}$ for each index i in \vec{X} . Ideally, if there is a one-to-one mapping between X_i and $Y_{h_j(i)}$, the value of X_i can be deduced as $g_j(i) \cdot Y_{h_j(i)}$. However, hash collision, where $Y_{h_j(i)}$ accumulates values from multiple counters, can occur. To mitigate this, Count Sketch reports the median of the values $g_j(i) \cdot Y_{h_j(i)}$ as its estimation. Including the $g_j(i)$ factor ensures that all potential collisions distribute symmetrically with a zero mean, thereby maintaining the unbiased nature of the estimation.

Now we can formally describe a Count Sketch-based compression algorithm that is homomorphic, though not yet lossless. The algorithm involves two phases to aggregate gradients. In the compression phase, each worker encodes the original gradient \vec{X} into a Count Sketch \vec{Y} , and transmits \vec{Y} to the existing aggregation API. In the recovery phase, each worker receives the aggregated Count Sketch $\sum \vec{Y}$, and estimate the parameters of $\sum \vec{X}$ from it.

3.2. Parallel Peeling: Lossless Recovery

To achieve the lossless property, we need to leverage an additional but very common feature of DNN gradient, called sparsity. This feature refers to the fact that most of the parameters are zero (Fei et al., 2021). By recording the locations of these zero parameters with a small index, we can compress only the non-zero parameters in the Count Sketch, making lossless compression possible.

We attain the lossless property by having each worker transmit an additional bitmap \vec{B} as the index, allocating one bit per parameter - for each bit, true indicates non-zero, while false indicates zero. It’s easy to find that the bitmap is also homomorphic in terms of bitwise-OR (\vee) operation, i.e., $\vec{B}(\sum \vec{X}) = \vee \vec{B}(\vec{X})$, as the aggregation of multiple non-zero parameters results in a non-zero value.⁴ Therefore, incorporating the compressed data with an additional bitmap, i.e., $\vec{S}(\vec{X}) = [\vec{Y}, \vec{B}]$, does not violate the homomorphic property, as long as we employ arithmetic summation to aggregate the Count Sketch and employ bitwise-OR to aggregate the bitmap, respectively.

The bitmap serves dual purposes. An obvious one is to directly indicate zero parameters and exactly report them. The second purpose is more intriguing: It enables a one-to-one mapping between the non-zero parameters and the Count Sketch.

Since we know the indexes of all non-zero parameters, we can figure out which indexes of \vec{Y} are mapped by only one non-zero parameter in \vec{X} . For these parameters, we

⁴Admitting that there’s a tiny probability that the result is zero, it doesn’t affect the correctness of our algorithm.

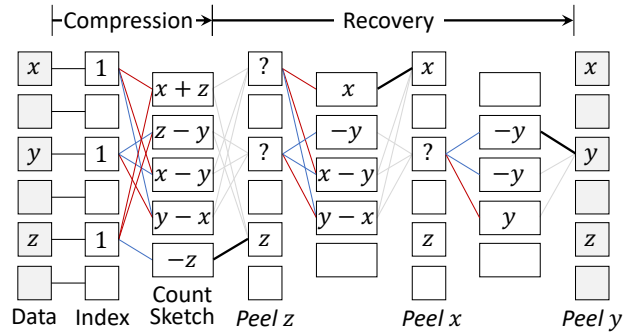


Figure 1. An example of our lossless homomorphic compression algorithm. In this example, three non-zero parameters - x , y , and z - identified by the index, are hashed and added to the Count Sketch. Ignoring the aggregation process and the parallel computation for the moment, to recover the data from the index and the Count Sketch, we first peel away z , since its value uniquely hashes to the bottom counter of the Count Sketch. Following this removal, x and y become eligible for peeling. This sequence allows for the lossless recovery of the entire gradient.

accurately recover their value X_i . Subsequently, we remove them from the bitmap by resetting the corresponding bit to zero. At the same time, we remove them from the Count Sketch by deducting $Y_{h_j(i)}$ by $g_j(i) \cdot X_i$. This process is akin to peeling away X_i from its insertion. After the two removal steps, there may emerge new peelable parameters, allowing us to continue the peeling process until \vec{X} is completely reconstructed or there are no more parameters that can be peeled.⁵ We show an example of our lossless homomorphic compression algorithm in Figure 1.

Theoretically, the peeling process is equivalent to finding two cores of a bipartite graph. Two closely related works include IBLT (Goodrich and Mitzenmacher, 2011) and Counter Braids (Lu et al., 2008). The distinction between these works and ours lies in the application focus: IBLT concentrates on compact key-value pair storage, whereas our approach supports homomorphic updates of values. Conversely, Counter Braids is tailored for network measurement with positive integers, while our method facilitates gradient aggregation for various data types.

According to the parallel peeling theory (Jiang et al., 2017), we can fully recover the aggregated data with a high probability of $1 - O(1/n)$, thus achieving the lossless property. This holds true provided that the size of the Count Sketch is at least γn where $\gamma = 1.23$ and n represents the number of non-zero parameters. Furthermore, it is proved that the parallel peeling process typically requires only $\log \log n + O(1)$ iterations to complete, and this figure can be easily optimized to $O(1)$ iterations in our algorithm by splitting the

⁵For the not peelable parameter, we use the Count Sketch to give an unbiased estimation.

Count Sketch into multiple blocks of fixed size, which is good news for the computation throughput.

3.3. Bloom Filter: High Compression Ratio

Though the design in §3.2 is already lossless, the bitmap presents a theoretical challenge: its size becomes significant, particularly for data types with small bit-width, when dealing with extremely high sparsity. To mitigate this issue, we substitute the bitmap with a probabilistic indexing structure called Bloom Filter (Bloom, 1970), thereby rendering the compression ratio asymptotically optimal.

Before delving into the details, let us reconsider the concept of lossless compression and establish a theoretical lower bound for the required storage space, denoted as S_{\min} . Suppose N is the total number of parameters of bit-width C and n is the number of non-zero parameters with values ranging from $[1..2^C - 1]$. For complete recovery of all parameters, a compressed data structure must include at least two types of information: an index of size S_1 bits identifying non-zero parameters and a table of S_2 bits recording their corresponding values. In scenarios where $S_1 = 0$, the index does not distinguish zero and non-zero values, necessitating the table to record all values as though the data were dense. Conversely, when $S_1 = N$, the index precisely identifies all zero and non-zero values, and the table only needs to record non-zero values. We therefore assume a balance between these extremes, with the index incorrectly identifying a certain portion, say ϵ , of zero parameters as non-zero. Consequently, the table records $\epsilon(N - n)$ redundant values. We denote ϵ as the false positive rate, and the aggregated data contains $\lambda n := N - n$ zero parameters. According to the chain rule theory of ChainedFilter (Li et al., 2023a), the overall space cost S satisfies

$$\begin{cases} S & \geq S_1 + S_2; \\ S_1 & \geq nf(\epsilon, \lambda) + o(n); \\ S_2 & \geq \log \left[\binom{Cn}{Cn(1+\epsilon\lambda)} \cdot (2^C - 1)^n \right] \\ & = Cnf(0, \epsilon\lambda) + n \log(2^C - 1) + o(n); \\ f(\epsilon, \lambda) & := f(0, \lambda) - f(0, \epsilon\lambda); \\ f(0, x) & := (x + 1)H\left(\frac{1}{x+1}\right), \forall x > 0; \\ H(x) & := -x \log x - (1 - x) \log(1 - x), \forall x \in (0, 1); \end{cases}$$

$$\Rightarrow S \geq (C - 1)nf(0, \epsilon\lambda) + nf(0, \lambda) + n \log(2^C - 1) + o(n) \geq nf(0, \lambda) + n \log(2^C - 1) := S_{\min}$$

Next, we illustrate how to asymptotically approach this bound S_{\min} using a probabilistic indexing structure called Bloom Filter (Bloom, 1970). A Bloom Filter is essentially a probabilistic bit array, with a size determined by the formula $\frac{n}{\ln 2} \log 1/\epsilon$ bits.⁶ In the compression phase, each worker

⁶In this context, n refers to the number of non-zero parameters

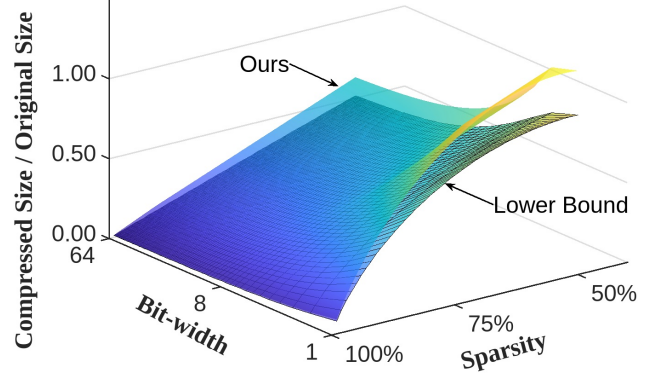


Figure 2. Theoretical compressed data size.

node constructs its Bloom Filter by hashing every non-zero parameter to $\log 1/\epsilon$ bits within the Bloom Filter and setting them to one. In the recovery phase, workers can approximate whether a parameter is non-zero by verifying that all the Bloom Filter’s corresponding bits are set to one. An indispensable nature of Bloom Filter to achieve the lossless property is that it never recognizes non-zero values as zero. This is because if any hashed bit of a parameter is zero, the parameter is zero. Otherwise, all the parameter bits would have been set to one when inserted. Another important property is that the Bloom Filter is homomorphic in terms of bitwise-OR (\vee) operation, *i.e.*, $\vec{B}(\sum \vec{X}) = \vee \vec{B}(\vec{X})$, so the aggregation API can merge the Bloom Filters like handling bitmaps.

By setting ϵ to $(\ln^2 2\gamma C\lambda)^{-1} \leq 1$, where γ is 1.23 mentioned in §3.2, we can figure out the overall space cost of the Count Sketch and the Bloom Filter S satisfies

$$\begin{cases} S & = S_1 + S_2; \\ S_1 & = \frac{n}{\ln 2} \log 1/\epsilon; \\ S_2 & = \gamma C(n + \epsilon(N - n)) = \gamma Cn(1 + \epsilon\lambda), \end{cases}$$

which is less than $1.6 \cdot S_{\min}$, asymptotically optimal in terms of compression ratio. An illustrative comparison between our algorithm and the theoretical lower bound is depicted in Figure 2.

3.4. Locality Optimization: High Computation Throughput

While our design described in §3.3 enables homomorphic and lossless compression with a high compression ratio, excessive hash computation and random memory access lead to frequent cache misses, limiting the system throughput. To address this problem, we propose to perform computations in a batched manner to enhance the locality of memory access, hence reducing cache misses.

and ϵ is the false positive rate mentioned in the previous paragraph. For simplicity, we don’t round formulas to the nearest integers.

Our solution is to group every $c = 1024$ consecutive parameter as a batch, where each batch shares the same index.⁷ Correspondingly, we reshape the original data \vec{X} , the count sketch \vec{Y} , and the index \vec{B} into matrices, denoted as \mathbf{X} , \mathbf{Y} and \mathbf{B} , respectively, each having a width of c . To ensure a random distribution of non-zero parameters across different columns of the Count Sketch \mathbf{Y} and the index \mathbf{B} , we introduce a random bias within the range $[0..c - 1]$ to rotate the order of parameters in one batch when mapping. For example, the 2nd, 3rd, and 4th parameters of \mathbf{X}_i could be mapped to the 22nd, 23rd, and 24th parameters of $\mathbf{Y}_{h_1(i)}$, the 122nd, 123rd, and 124th parameters of $\mathbf{Y}_{h_2(i)}$, and the 1022nd, 1023rd, and 1st parameters of $\mathbf{Y}_{h_3(i)}$, respectively. This approach guarantees that, as long as the Count Sketch size $\|\mathbf{Y}\|_0 \geq \gamma \|\mathbf{X}\|_0$ where $\gamma = 1.23$, full recovery of \mathbf{X} is achievable with a high probability of $1 - O(\|\mathbf{X}\|_0^{-1})$, thereby preserving the lossless property.

4. Evaluation

We implement and integrate our homomorphic compression algorithm into the NVIDIA Collective Communications Library (NCCL) and the ATP in-network aggregation framework (Lao et al., 2021) in PyTorch (Paszke et al., 2019). We compare our algorithm with two baselines: (1) NCCL AllReduce aggregation that represents worker-level aggregation and (2) ATP’s in-network aggregation that represents in-network aggregation without compression.

We evaluate our algorithm while training the following models of varying sizes and gradient sparsity (Table 1): NCF (He et al., 2017) with the ml-25m (Harper and Konstan, 2015) dataset, LSTM (Hochreiter and Schmidhuber, 1997) with the GBW (Chelba et al., 2013) dataset, VGG19 (Simonyan and Zisserman, 2014) with the CIFAR-10 (Krizhevsky et al., 2009) dataset, and BERT-base (Devlin et al., 2018) with the SQuAD (Rajpurkar et al., 2016) dataset.

We use two separate clusters to evaluate each implementation due to hardware constraints in our testbed.

(1) **NCCL-based implementation:** The cluster consists of four GPU servers, each equipped with two NVIDIA A100 GPUs with 80 GB memory, interconnected via a 100 Gbps switch. GPUs on the same server are interconnected by NVIDIA’s NVLink, and routed with a regular switch.

(2) **ATP-based implementation:** The cluster has an Intel Tofino programmable switch that runs ATP-based in-network aggregation. It consists of three GPU servers, each equipped with an NVIDIA GeForce RTX 2080 GPU with 12 GB memory, interconnected by a 10 Gbps network.

⁷We choose c based on the GPU architecture we use in our experiments. Specifically, the NVIDIA GPUs we use support up to 1024 threads per GPU block.

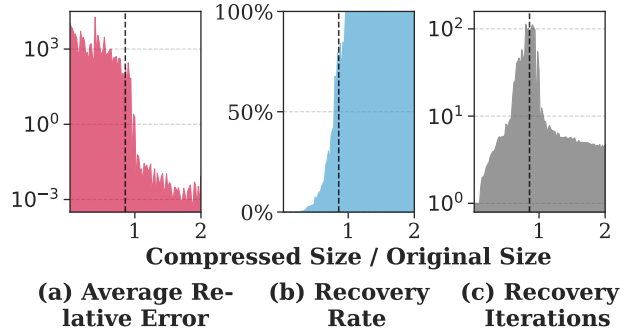


Figure 3. Average relative error, recovery rate, and iterations.

4.1. Microbenchmarks

4.1.1. IMPACT OF COMPRESSION ON TRAINING ACCURACY

To evaluate the losslessness of our algorithm, we measure the recovery accuracy when using our algorithm in training the VGG19 model on a single worker equipped with one GPU (*i.e.*, no aggregation across GPUs). We perform this experiment to demonstrate the recovery performance of our algorithm by decompressing the parameters immediately after compressing them.

We first evaluate the recovery accuracy in each iteration using the following three metrics:

(1) **Average relative error:** It is an average of the absolute values of the relative differences between original and decompressed parameters.

(2) **Recovery rate:** It quantifies the proportion of parameters that are successfully recovered using the peeling theory (§3.2). A compression algorithm is lossless if it achieves a 100% recovery rate, meaning all parameters are successfully recovered. Note that losslessly recovered data may not exactly match the original data. This discrepancy is primarily due to the inherent imprecision of floating-point computation. The lossless property only ensures that if the precision of floating points approaches infinity, the recovered data would perfectly align with the original data.

(3) **Recovery iterations:** It denotes the number of iterations required to recover all possible parameters. Although not a measure of accuracy, we include it to demonstrate the property that the recovery process typically finishes within $\log \log n + O(1) = 4.7 + O(1)$ iterations (§3.2).

We vary the compressed data size from 2% to 200% of the original data size.⁸ Figure 3 shows the results that once

⁸It may seem odd, but sometimes the compressed data size can be larger than the original data size. This is because when the original data is already dense, compression could actually increase data size by adding redundant information such as indexes in the

Table 1. DNN models used in our evaluation.

Model	Task	Dataset	Batch Size	Number of Parameters	Average Sparsity
NCF	Recommendation System	ml-25m	1024	29.7 Million	98.9%
LSTM	Language Modeling	GBW	64	426 Million	94.5%
VGG19	Image Classification	CIFAR-10	128	140 Million	30.4%
BERT-base	Question Answering	SQuAD	8	109 Million	20.8%

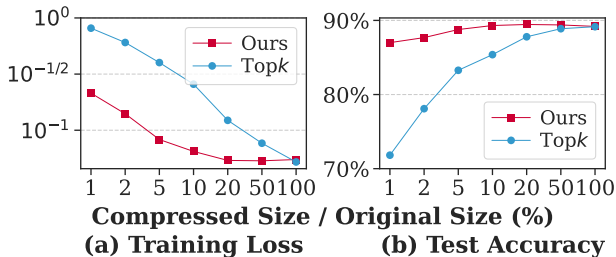


Figure 4. Training loss and test accuracy.

the compressed data size surpasses a certain threshold ($\gamma \times (1 - \text{Sparsity}) = 1.23 \times (1 - 30.4\%) = 85.6\%$ of the original data size, see the vertical dotted lines), the average relative error rapidly approaches near zero (Figure 3 (a)) and the recovery rate surges to 100% (Figure 3 (b)). We also observe a decrease in recovery iterations, indicating a higher throughput of the recovery process (Figure 3 (c)).

Next, we measure the training loss and test accuracy when training the VGG19 model until the model get converged while varying compression ratios. Figure 4 shows the results. As the compression ratios decreases (*i.e.*, higher recovery rate), training loss decreases while test accuracy increases. This demonstrates why the lossless compression is beneficial even if a lossy approach can preserve convergence. We also compare our algorithm with the vanilla Topk compression, showing that our algorithm outperforms with the same compression ratio. This is because our algorithm provides an unbiased estimation for the near-zero parameters, while the Topk algorithm simply quantifies them to zero.⁹

4.1.2. IMPACT OF COMPRESSION ON AGGREGATION THROUGHPUT

To evaluate the impact of the compression ratio on the aggregation performance, we measure the aggregation throughput defined as the volume of aggregated gradients in gigabits per second (*i.e.*, Gbps) while varying the compressed data size from 2% to 100% of the original data size.¹⁰ Note

⁹While prior work aims to compensate for the loss of precision by accumulating and transmitting near-zero values every few iterations (Lin et al., 2017), it is orthogonal to our solution.

¹⁰In our cluster with 8 GPUs, aggregating 8×100 gigabits gradients in one second is counted as 100 Gbps, not 800 Gbps.

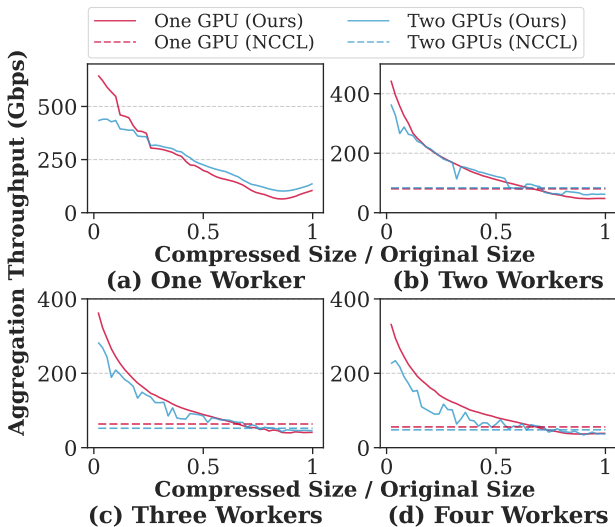


Figure 5. Aggregation throughput of NCCL-based experiments.

that the aggregation throughput only takes into account the compression, aggregation, and recovery processes. Other training processes, such as forward and backward propagation, are not included in the aggregation throughput. In this experiment, we train models using one to four workers, each utilizing either one or two GPUs.

Figure 5 depicts the results. The result from a single worker with a single GPU case shows the throughput of the compression and decompression processes (Figure 5 (a)). At small compressed data sizes, the throughput reaches up to 646 Gbps. As the compressed data size increases, the throughput decreases to 64.7 Gbps, mainly due to an increase in memory access and recovery iterations. Interestingly, when the compressed data size reaches 100% of the original data size (*i.e.*, no compression), the throughput increases again. This is likely because of the reduction in recovery iterations. When using a single worker with two GPUs, if the compressed data size is smaller, the throughput is lower compared to using a single GPU, probably due to the NVLink throughput limit. However, as the compressed data size increases, the dual GPU configuration becomes faster due to the distributed load of the recovery process.

Our algorithm exhibits significant improvements in comparison to the NCCL baseline when multiple workers are

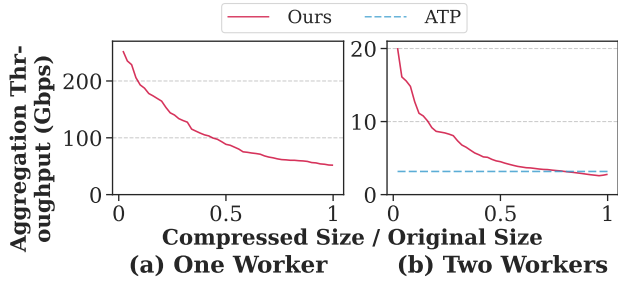


Figure 6. Aggregation throughput of ATP-based experiments.

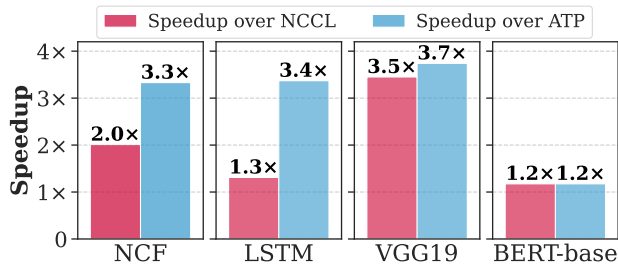


Figure 7. Per iteration speedup. Note that comparing between the red and blue bars would be meaningless because these experiments are conducted on different clusters.

employed (Figure 5 (b-d)). When compressed data sizes are small, the algorithm can achieve speedups of up to $4.97\times$ (4 Workers, 1 GPU) compared to the baseline. However, when data sizes are larger than 60% of the original data size, the algorithm may experience a reduction in aggregation throughput due to high computational overhead.

In ATP-based in-network aggregation experiments, we train models with one or two workers¹¹ equipped with a single GPU each (Figure 6). Our findings were similar to those of the NCCL-based experiments, with the maximum specific speedup reaching up to $6.33\times$.

4.2. End-to-end Evaluation

To evaluate the end-to-end performance of our algorithm, we measure per-iteration and overall speedups. Here, we fix the compression data size to 10% of the original data size. In NCCL-based experiments, we employ four workers, each with two GPUs. In ATP-based experiments, we utilized two workers, each with a single GPU.

Figure 7 shows the per-iteration speedup achieved by our algorithm. We find that on NCF, LSTM, VGG19 and BERT-base models, our algorithm achieves speedup of $2.01\times$, $1.31\times$, $3.45\times$, and $1.17\times$ over the NCCL baseline, and accelerates $3.33\times$, $3.37\times$, $3.74\times$, and $1.17\times$ over the ATP

¹¹Of the three available GPU machines in our testbed, one is used as a parameter server, leaving two available workers.

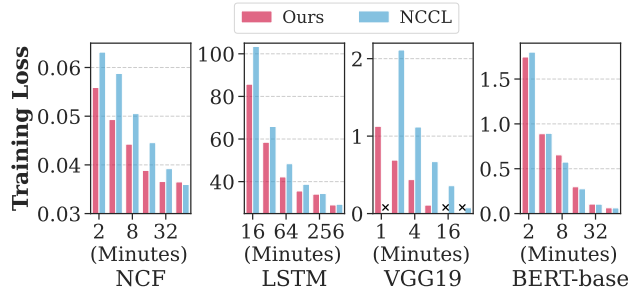


Figure 8. Overall training loss over time.

baseline. The proportion of computation to communication overhead influences this result. Usually, when communication makes up a larger proportion, our algorithm tends to accelerate more noticeably. It is worth noting that for models such as NCF and LSTM, whose gradient is very sparse, the per-iteration speedup can be approximately the overall speedup. This is because in these cases, our algorithm is verified to recover gradients without loss (*i.e.*, with a 100% recovery rate). However, for VGG19 and BERT-base, the situation is different because our compression is lossy, requiring more training iterations to converge.

To evaluate the overall speedups, we measure the training loss.¹² The experimental results based on NCCL are presented in Figure 8. We compare the training loss achieved by our algorithm and the NCCL baseline over the same amount of training time. On NCF, LSTM and VGG19 models, our algorithm significantly speeds up the training process. Even on BERT-base, which has a non-sparse gradient, our algorithm perform comparably to the NCCL baseline. We observe the same results from ATP-based experiments.

5. Conclusion

In this paper, we present a lossless homomorphic algorithm that combines worker-level compression and in-network aggregation to address the communication bottlenecks in DNN training. It uses dual homomorphic structures to create compressed data that preserves all information and leverages algorithms in the area of random graph to recover the original data without losing accuracy. It provides an optimal compression ratio and computational complexity. Our evaluation shows that it improves the aggregation throughput by up to $6.33\times$ and achieves a $3.74\times$ speedup in per-iteration training speed in distributed training tasks. We believe that the theories and techniques presented in this paper will inspire more innovative works in the ML community.

¹²The loss functions vary across training tasks. Specifically, we employ perplexity for NCF, PyTorch’s BCEWithLogitsLoss() for LSTM, and PyTorch’s CrossEntropyLoss() for both VGG19 and BERT-base.

References

- Mike Barnett, Lance Shuler, Robert van De Geijn, Satya Gupta, David G Payne, and Jerrell Watts. Interprocessor collective communication library (intercom). In *Proceedings of IEEE Scalable High Performance Computing Conference*, pages 357–364. IEEE, 1994.
- Tal Ben-Nun and Torsten Hoefler. Demystifying parallel and distributed deep learning: An in-depth concurrency analysis. *ACM Computing Surveys (CSUR)*, 52(4):1–43, 2019.
- Burton H Bloom. Space/time trade-offs in hash coding with allowable errors. *Communications of the ACM*, 13(7):422–426, 1970.
- Léon Bottou, Frank E Curtis, and Jorge Nocedal. Optimization methods for large-scale machine learning. *SIAM review*, 60(2):223–311, 2018.
- Tom Brown, Benjamin Mann, Nick Ryder, Melanie Subbiah, Jared D Kaplan, Prafulla Dhariwal, Arvind Neelakantan, Pranav Shyam, Girish Sastry, Amanda Askell, et al. Language models are few-shot learners. *Advances in neural information processing systems*, 33:1877–1901, 2020.
- Ernie Chan, Marcel Heimlich, Avi Purkayastha, and Robert Van De Geijn. Collective communication: theory, practice, and experience. *Concurrency and Computation: Practice and Experience*, 19(13):1749–1783, 2007.
- Moses Charikar, Kevin Chen, and Martin Farach-Colton. Finding frequent items in data streams. In *International Colloquium on Automata, Languages, and Programming*, pages 693–703. Springer, 2002.
- Ciprian Chelba, Tomas Mikolov, Mike Schuster, Qi Ge, Thorsten Brants, Phillipp Koehn, and Tony Robinson. One billion word benchmark for measuring progress in statistical language modeling. *arXiv preprint arXiv:1312.3005*, 2013.
- Tim Dettmers. 8-bit approximations for parallelism in deep learning. *arXiv preprint arXiv:1511.04561*, 2015.
- Jacob Devlin, Ming-Wei Chang, Kenton Lee, and Kristina Toutanova. Bert: Pre-training of deep bidirectional transformers for language understanding. *arXiv preprint arXiv:1810.04805*, 2018.
- Jiawei Fei, Chen-Yu Ho, Atal N Sahu, Marco Canini, and Amedeo Sapia. Efficient sparse collective communication and its application to accelerate distributed deep learning. In *Proceedings of the 2021 ACM SIGCOMM 2021 Conference*, pages 676–691, 2021.
- Aoxiang Feng, Dezun Dong, Fei Lei, Junchao Ma, Enda Yu, and Ruiqi Wang. In-network aggregation for data center networks: A survey. *Computer Communications*, 198:63–76, 2023.
- Nadeen Gebara, Manya Ghobadi, and Paolo Costa. In-network aggregation for shared machine learning clusters. *Proceedings of Machine Learning and Systems*, 3:829–844, 2021.
- Michael T Goodrich and Michael Mitzenmacher. Invertible bloom lookup tables. In *2011 49th Annual Allerton Conference on Communication, Control, and Computing (Allerton)*, pages 792–799. IEEE, 2011.
- Udit Gupta, Carole-Jean Wu, Xiaodong Wang, Maxim Nau-mov, Brandon Reagen, David Brooks, Bradford Cottel, Kim Hazelwood, Mark Hempstead, Bill Jia, et al. The architectural implications of facebook’s dnn-based personalized recommendation. In *2020 IEEE International Symposium on High Performance Computer Architecture (HPCA)*, pages 488–501. IEEE, 2020.
- F Maxwell Harper and Joseph A Konstan. The movielens datasets: History and context. *Acm transactions on interactive intelligent systems (tiis)*, 5(4):1–19, 2015.
- Kaiming He, Xiangyu Zhang, Shaoqing Ren, and Jian Sun. Deep residual learning for image recognition. In *Proceedings of the IEEE conference on computer vision and pattern recognition*, pages 770–778, 2016.
- Xiangnan He, Lizi Liao, Hanwang Zhang, Liqiang Nie, Xia Hu, and Tat-Seng Chua. Neural collaborative filtering. In *Proceedings of the 26th international conference on world wide web*, pages 173–182, 2017.
- Sepp Hochreiter and Jürgen Schmidhuber. Long short-term memory. *Neural computation*, 9(8):1735–1780, 1997.
- Nikita Iykin, Daniel Rothchild, Enayat Ullah, Ion Stoica, Raman Arora, et al. Communication-efficient distributed sgd with sketching. *Advances in Neural Information Processing Systems*, 32, 2019.
- Jaehee Jang, Byungook Na, and Sungroh Yoon. Homomorphic parameter compression for distributed deep learning training. *arXiv preprint arXiv:1711.10123*, 2017.
- Jiayang Jiang, Michael Mitzenmacher, and Justin Thaler. Parallel peeling algorithms. *ACM Transactions on Parallel Computing (TOPC)*, 3(1):1–27, 2017.
- Yimin Jiang, Yibo Zhu, Chang Lan, Bairen Yi, Yong Cui, and Chuanxiong Guo. A unified architecture for accelerating distributed {DNN} training in heterogeneous {GPU/CPU} clusters. In *14th USENIX Symposium on Operating Systems Design and Implementation (OSDI 20)*, pages 463–479, 2020.

- Alex Krizhevsky, Geoffrey Hinton, et al. Learning multiple layers of features from tiny images. 2009.
- ChonLam Lao, Yanfang Le, Kshiteej Mahajan, Yixi Chen, Wenfei Wu, Aditya Akella, and Michael Swift. {ATP}: In-network aggregation for multi-tenant learning. In *18th USENIX Symposium on Networked Systems Design and Implementation (NSDI 21)*, pages 741–761, 2021.
- Haoyu Li, Qizhi Chen, Yixin Zhang, Tong Yang, and Bin Cui. Stingy sketch: a sketch framework for accurate and fast frequency estimation. *Proceedings of the VLDB Endowment*, 15(7):1426–1438, 2022.
- Haoyu Li, Liuhui Wang, Qizhi Chen, Jianan Ji, Yuhan Wu, Yikai Zhao, Tong Yang, and Aditya Akella. Chainedfilter: Combining membership filters by chain rule. *Proceedings of the ACM on Management of Data*, 1(4):1–27, 2023a.
- Minghao Li, Ran Ben Basat, Shay Vargafit, ChonLam Lao, Kevin Xu, Xinran Tang, Michael Mitzenmacher, and Minlan Yu. Thc: Accelerating distributed deep learning using tensor homomorphic compression. *arXiv preprint arXiv:2302.08545*, 2023b.
- Mu Li, David G Andersen, Jun Woo Park, Alexander J Smola, Amr Ahmed, Vanja Josifovski, James Long, Eugene J Shekita, and Bor-Yiing Su. Scaling distributed machine learning with the parameter server. In *11th USENIX Symposium on operating systems design and implementation (OSDI 14)*, pages 583–598, 2014.
- Shigang Li and Torsten Hoefler. Near-optimal sparse allreduce for distributed deep learning. In *Proceedings of the 27th ACM SIGPLAN Symposium on Principles and Practice of Parallel Programming*, pages 135–149, 2022.
- Yujun Lin, Song Han, Huizi Mao, Yu Wang, and William J Dally. Deep gradient compression: Reducing the communication bandwidth for distributed training. *arXiv preprint arXiv:1712.01887*, 2017.
- Yi Lu, Andrea Montanari, Balaji Prabhakar, Sarang Dharmapurikar, and Abdul Kabbani. Counter braids: a novel counter architecture for per-flow measurement. *ACM SIGMETRICS Performance Evaluation Review*, 36(1): 121–132, 2008.
- Liang Luo, Jacob Nelson, Luis Ceze, Amar Phanishayee, and Arvind Krishnamurthy. Parameter hub: a rack-scale parameter server for distributed deep neural network training. In *Proceedings of the ACM Symposium on Cloud Computing*, pages 41–54, 2018.
- Paulius Micikevicius, Sharan Narang, Jonah Alben, Gregory Diamos, Erich Elsen, David Garcia, Boris Ginsburg, Michael Houston, Oleksii Kuchaiev, Ganesh Venkatesh, et al. Mixed precision training. *arXiv preprint arXiv:1710.03740*, 2017.
- Heng Pan, Penglai Cui, Ru Jia, Penghao Zhang, Leilei Zhang, Ye Yang, Jiahao Wu, Jianbo Dong, Zheng Cao, Qiang Li, et al. Libra: In-network gradient aggregation for speeding up distributed sparse deep training. *arXiv preprint arXiv:2205.05243*, 2022.
- Adam Paszke, Sam Gross, Francisco Massa, Adam Lerer, James Bradbury, Gregory Chanan, Trevor Killeen, Zeming Lin, Natalia Gimelshein, Luca Antiga, et al. Pytorch: An imperative style, high-performance deep learning library. *Advances in neural information processing systems*, 32, 2019.
- Pitch Patarasuk and Xin Yuan. Bandwidth optimal allreduce algorithms for clusters of workstations. *Journal of Parallel and Distributed Computing*, 69(2):117–124, 2009.
- Pranav Rajpurkar, Jian Zhang, Konstantin Lopyrev, and Percy Liang. Squad: 100,000+ questions for machine comprehension of text. *arXiv preprint arXiv:1606.05250*, 2016.
- Cédric Renggli, Saleh Ashkboos, Mehdi Aghagolzadeh, Dan Alistarh, and Torsten Hoefler. Sparcml: High-performance sparse communication for machine learning. In *Proceedings of the International Conference for High Performance Computing, Networking, Storage and Analysis*, pages 1–15, 2019.
- Amedeo Sapio, Marco Canini, Chen-Yu Ho, Jacob Nelson, Panos Kalnis, Changhoon Kim, Arvind Krishnamurthy, Masoud Moshref, Dan Ports, and Peter Richtárik. Scaling distributed machine learning with {In-Network} aggregation. In *18th USENIX Symposium on Networked Systems Design and Implementation (NSDI 21)*, pages 785–808, 2021.
- Frank Seide, Hao Fu, Jasha Droppo, Gang Li, and Dong Yu. 1-bit stochastic gradient descent and its application to data-parallel distributed training of speech dnns. In *Fifteenth annual conference of the international speech communication association*, 2014.
- Jaime Sevilla, Lennart Heim, Anson Ho, Tamay Besiroglu, Marius Hobbhahn, and Pablo Villalobos. Compute trends across three eras of machine learning. In *2022 International Joint Conference on Neural Networks (IJCNN)*, pages 1–8. IEEE, 2022.
- Shaohuai Shi, Qiang Wang, Kaiyong Zhao, Zhenheng Tang, Yuxin Wang, Xiang Huang, and Xiaowen Chu. A distributed synchronous sgd algorithm with global top-k sparsification for low bandwidth networks. In *2019 IEEE 39th International Conference on Distributed Computing Systems (ICDCS)*, pages 2238–2247. IEEE, 2019.

- Karen Simonyan and Andrew Zisserman. Very deep convolutional networks for large-scale image recognition. *arXiv preprint arXiv:1409.1556*, 2014.
- Peng Sun, Wansen Feng, Ruobing Han, Shengen Yan, and Yonggang Wen. Optimizing network performance for distributed dnn training on gpu clusters: Imagenet/alexnet training in 1.5 minutes. *arXiv preprint arXiv:1902.06855*, 2019.
- Linnan Wang, Wei Wu, Junyu Zhang, Hang Liu, George Bosilca, Maurice Herlihy, and Rodrigo Fonseca. Fft-based gradient sparsification for the distributed training of deep neural networks. In *Proceedings of the 29th International Symposium on High-Performance Parallel and Distributed Computing*, pages 113–124, 2020.
- Ze Qin Wang, Ming Wen, Yuedong Xu, Yipeng Zhou, Jessie Hui Wang, and Liang Zhang. Communication compression techniques in distributed deep learning: A survey. *Journal of Systems Architecture*, page 102927, 2023.
- Wei Wen, Cong Xu, Feng Yan, Chunpeng Wu, Yandan Wang, Yiran Chen, and Hai Li. Terngrad: Ternary gradients to reduce communication in distributed deep learning. *Advances in neural information processing systems*, 30, 2017.
- Wenpeng Yin, Katharina Kann, Mo Yu, and Hinrich Schütze. Comparative study of cnn and rnn for natural language processing. *arXiv preprint arXiv:1702.01923*, 2017.